Big Bang Nucleosynthesis Limits and Relic Gravitational-Wave Detection Prospects

Tina Kahniashvili[1,2,3,*] Emma Clarke[1,†] Jonathan Stepp[1,‡] and Axel Brandenburg[4,5,2,1,§]

[1]*McWilliams Center for Cosmology and Department of Physics, Carnegie Mellon University, Pittsburgh, Pennsylvania 15213, USA*
[2]*School of Natural Sciences and Medicine, Ilia State University, 0194 Tbilisi, Georgia*
[3]*Abastumani Astrophysical Observatory, Tbilisi GE-0179, Georgia*
[4]*Nordita, KTH Royal Institute of Technology and Stockholm University, 10691 Stockholm, Sweden*
[5]*The Oskar Klein Centre, Department of Astronomy, Stockholm University, AlbaNova, SE-10691 Stockholm, Sweden*

We revisit the big bang nucleosynthesis limits on primordial magnetic fields and/or turbulent motions accounting for the decaying nature of turbulent sources between the time of generation and big bang nucleosynthesis. This leads to larger estimates for the gravitational wave signal than previously expected. We address the detection prospects through space-based interferometers and pulsar timing arrays or astrometric missions for gravitational waves generated around the electroweak and quantum chromodynamics energy scale, respectively.

Gravitational radiation from the early universe propagates almost freely throughout the universe's expansion and primordial gravitational waves (GWs) reflect a precise picture of the very early universe. Detection of these GWs is a promising tool that would open new avenues to understand physical processes at energy scales inaccessible to high energy particle physics experiments but accessible to astrophysical observation [1].

There are several milestones of modern cosmology, proven through cosmic microwave background (CMB) anisotropies and large scale structure statistics. In particular, the light element abundances allow us to reconstruct the picture of big bang nucleosynthesis (BBN), but leave several puzzles prior to BBN (matter-antimatter asymmetry, dynamics of the universe at the very beginning, nature of dark matter, etc.) unsolved. These unknowns will be reflected in the variety of relic GW characteristics, including not only the strength of the signal and its spectral shape, but also its polarization. Indeed detection of GW polarization is a unique tool to test fundamental symmetries at these extremely high energies. If GWs originated from parity violating sources in the early universe, they will be circularly polarized and, unlike the CMB, GW polarization will exist at the basic background and *not just the perturbation* level; see Ref. [2] for pioneering work and see Refs. [3–8] for recent studies. This is analogous to the GWs produced via Chern-Simons coupling [9,10]. If detected, the GW polarization can be a *direct* measure of the deviations from the standard model (SM) [11–13]. One of the major goals of this Letter is to determine whether these circularly polarized GWs and their polarization are potentially detectable in the upcoming early-universe GW observation missions [14]. The strategy to detect the stochastic GW polarization is based on anisotropy [15] induced, for example, through our proper motion [16,17]. Despite promising detection prospects for stochastic GWs through pulsar timing arrays (PTAs), which are potentially sensitive to GWs generated around the quantum chromodynamic (QCD) energy scale, detection of the polarization degree remains problematic.

BBN data (based on light element abundances [18]) impose an upper limit on the universe's expansion rate, e.g., the Hubble parameter, $H = d \ln a / dt_{\mathrm{phys}}$ (with physical time t_{phys} and scale factor a), and correspondingly, on additional relativistic species such as massless (or ultra-relativistic) hypothetical particles, early stage dark energy (or any bosonic massless field), dark radiation, electromagnetic fields or early-universe plasma motions (turbulence), relic GWs, etc. [21–27]. Conventionally, the energy density of these additional relativistic components is characterized in terms of the *effective number of relativistic species*, N_{eff}. The SM predicts for neutrino species $N_{\mathrm{eff}}^{(\nu)} = 3.046$, which is slightly larger than 3 because neutrinos did not decouple instantaneously and were still able to interact with electrons and positrons near electron-positron annihilation [28]. Other additional relativistic components contribute $\Delta N_{\mathrm{eff}} = N_{\mathrm{eff}} - N_{\mathrm{eff}}^{(\nu)}$ to this *effective* neutrino count. Notably, the presence of additional relativistic components does not spoil the time dependence of the scale factor during the radiation-dominated epoch, but it does affect the Hubble parameter and Hubble time scale, H^{-1}. The joint analysis of CMB measurements and BBN light element abundances put $N_{\mathrm{eff}} = 2.862 \pm 0.306$ at 95% confidence [29]. Using the upper bound of this error interval ($N_{\mathrm{eff}} = 3.168$), we express the maximum ratio of

additional components of energy density $\rho_{\rm add}$ to the radiation energy density $\rho_{\rm rad}$ at the BBN temperature as $\rho_{\rm add}/\rho_{\rm rad} \simeq 0.0277 \cdot (\Delta N_{\rm eff}/0.122)$, normalized around $\Delta N_{\rm eff} = 0.122$. The maximum value of this ratio is limited by the combined CMB and BBN data. We note that this upper bound coincides with the constraint on the GW contribution to the radiation energy density found in Ref. [30] using CMB and BBN data combined with limits from NANOGrav and late-time measurements of the expansion history. Interestingly, the light element abundances (with the bounds on $N_{\rm eff}$) impose limits on the lepton asymmetry in the universe [31] that might result in primordial chiral magnetic fields [32] and correspondingly serve as a source for polarized GWs [8].

In this Letter we address the BBN bounds from the point of view of early-universe anisotropic stress (namely, primordial magnetic fields and turbulent sources) and the induced GW signal. Inhomogeneous magnetic fields are known to affect the primordial lithium abundance [33]. Here, however, we are particularly interested in the strength, the spectral shape, and the polarization degree of the induced GWs. Violent processes in the early universe might lead to the development of turbulence. In particular, first order electroweak (EW) and QCD phase-transition bubble collisions and nucleation might lead to turbulent plasma motions [34–37], or, alternatively, turbulence can be induced by primordial magnetic fields coupled to the cosmological plasma [38–42]. The stochastic GW background from these turbulent sources has been studied for decades now; see Refs. [37,43,44] for pioneering works and Ref. [45] for a review and references therein.

Both analytical and numerical studies suggest that a strong enough gravitational radiation signal (when and if the total energy density of the source is a substantial fraction of the total (radiation) energy density, $\rho_{\rm rad}$, at the moment of the GW generation, characterized by the temperature, $T_\star$, and the number of relativistic degrees of freedom, $g_\star$, where here and below an asterisk denotes the generation moment) is detectable by space-based missions, such as the Laser Interferometer Space Antenna (LISA) (for GWs generated around the EW energy scale) [45], or by PTAs, such as NANOGrav [46], and astrometric missions such as GAIA [47] (for GWs generated around the QCD energy scale). Notably, the NANOGrav Collaboration recently announced strong evidence for a stochastic GW signal [46] that might be associated with primordial sources [48]. On the other hand, when estimating the strength of the GW signal, the maximum allowed source energy density was assumed to be determined by the BBN bounds discussed above (i.e., not exceeding a few percent of the total radiation energy, i.e., $\mathcal{E}_{\rm turb} = \zeta\rho_{\rm rad}$ with the parameter ζ being in general time dependent and being a few percent at BBN).

Because of weak coupling between gravity and matter (i.e., the smallness of Newton's constant G), the GW generation from any turbulent source is characterized by low efficiency and, consequently, the ratio ζ of turbulent source energy density to the total radiation energy is not affected by the emission of gravitational radiation. In other words, the energy radiated in GWs will not induce substantial damping of the turbulent energy density. Moreover, if turbulent decay processes are discarded (i.e., velocity and magnetic fields are "frozen-in" to the primordial plasma), ζ is unchanged during the radiation-dominated epoch. Applying this logic to the BBN bounds, the few percent limit was applied *a priori* to much earlier time scales when GWs were generated. As it was seen in simulations [7,49], the GW energy density reaches a maximum and stays unchanged after a short time. Thus, only ζ at *the moment of the source activation* (i.e., GW generation) matters.

In the case of decaying turbulence, the situation is different: ζ is time dependent and the decay rate is determined by the specific model of turbulence. Decaying turbulence leads to a power-law decay $\mathcal{E}_{\rm turb}(t) \propto (t/t_\star)^{-p}$, and a growth of the correlation length $\xi_{\rm turb}$ by an inverse cascade mechanism such that $\xi_{\rm turb} \propto (t/t_\star)^q$, where $t = \int dt_{\rm phys}/a$ is the conformal time and the parameters p and q depend on the properties of the turbulence (e.g., in helical turbulence $p = q = 2/3$, while for nonhelical magnetically dominated turbulence $p = 1$ and $q = 1/2$, but other variants are possible). The scaling exponent q may reflect the presence of an underlying conservation law (helicity conservation, Loitsiansky integral) and is also determined by the nature of turbulence (kinetically or magnetically dominated). The combined values of p and q for a particular process can be summarized by the parameter $\beta = p/q - 1$, which characterizes the decay of the spectral peak of magnetic energy [50]. Partially helical magnetic fields are also described by their fractional helicity, i.e., the ratio of the magnetic helicity to its maximal value, $\epsilon_{M,\star} < 1$. Because of this decay, the BBN bound allows larger values of ζ at the moment of GW generation, making the GW signal stronger. The maximum allowed energy density of turbulent sources that satisfy the BBN limits will be different at the EW and QCD energy scales (EW turbulence has a longer decay period, allowing higher values for the initial energy density that still satisfies the BBN bounds).

Figure 1 shows the bounds on the strength of the magnetic fields at their generation (EW or QCD scales) determined such that the strength does not exceed the upper limit of the comoving field strength at BBN [51] and is above the lower observational bounds on the field strength at recombination. We see that allowed values for the magnetic fields at the moment of generation (upper left end of the lines) are not constrained to microgauss field strength, as it was claimed previously based on BBN bounds without accounting for decaying turbulence [52]. In fact, if we were previously considering an Alfvén speed
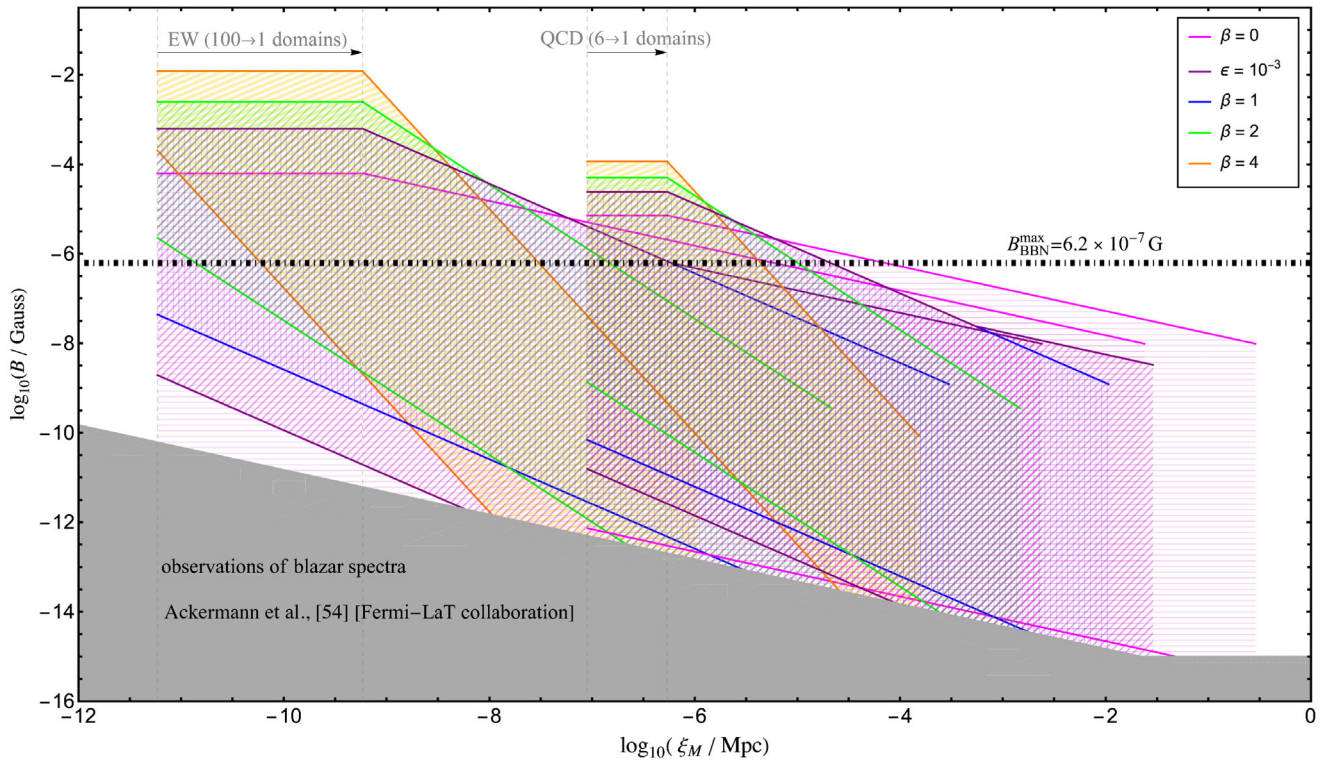
FIG. 1. Possible turbulent evolution of the comoving magnetic field strength B (decaying with time) and correlation length ξ_M (increasing with time) from generation at the EW and QCD scales in the cases of fully helical ($\beta = 0$), nonhelical ($\beta = 1, 2, 4$), and partially helical (with $\epsilon_{M,\star} = 10^{-3}$) MHD turbulence. Upper limits on the correlation length are determined by the size of the horizon and number of domains (bubbles) at generation, ranging from 1 to 6 (at QCD) or 100 (at EW), depending on the phase transition modeling. Lines terminate (on the right) at recombination ($T = 0.25$ eV). The upper limit of the comoving field strength at BBN ($T = 0.1$ MeV) is indicated by the black dot-dashed line. Regimes excluded by observations of blazar spectra [54] are marked in gray. The hatched regions correspond to possible trajectories bounded by an (upper) limit from BBN and a (lower) limit from the blazar spectra.

v_A or characteristic velocities of 0.2–0.3 (in units of the speed of light), the new limits possibly imply $v_A \to 1$ [49]. Obviously, in this case we deal with relativistic turbulence that might be characterized by different decay laws or efficiency to generate GWs. However, recent relativistic turbulence numerical simulations [53] show that the basic properties of turbulence decay are preserved, including nonhelical inverse cascading. Also, following arguments of Ref. [43], the nonrelativistic description of turbulent sources results in an underestimation of the signal.

Below we present the first simulations of the GW signal from such strong turbulence sources. We use PENCIL CODE [55,56] to simulate magnetohydrodynamic (MHD) turbulence in the early universe by computing the stochastic GW background and relic magnetic fields [49]. Turbulence is driven by applying an electromagnetic force that is δ-correlated in time and has the desired spatial spectrum. We vary the forcing strength and adjust the viscosity such that the smallest length scales in the simulation are sufficiently well resolved to dissipate the injected energy near the highest available wave number. We perform runs for the QCD and EW energy scales; see Ref. [51] for a table summarizing the eight runs presented in this Letter.

The GW detection prospects are strongly affected by the characteristic frequency ranges and thus the energy-containing wave number of the source. More precisely, the GW spectrum peaks at the comoving angular frequency $\omega_{\text{peak}} = (2\pi f_{\text{peak}}) = 2k_0$, where k_0 is the initial peak wave number of the source energy density spectrum (in natural units $c = 1$). The inertial wave number is determined by the turbulent eddy size ($k_0 = 2\pi/L$), and if we assume that turbulence arises from phase transitions, the eddy size may be associated with the bubble size [57]. Independently of the nature the turbulence, the typical length scale is limited by the Hubble scale. In what follows, we use the characteristic wave number k_0 normalized by the Hubble wave number $H_\star$.

The energy density of early-universe turbulent sources is determined by the efficiency of converting the available radiation energy into turbulent energy. In the case of first-order phase transitions, it can be expressed in the terms of the parameter $\alpha = \rho_{\text{vac}}/\rho_{\text{rad}} = 4\rho_{\text{vac}}/3(\rho + P)$ (with ρ and P being the plasma energy density and pressure, respectively)—the ratio between the latent heat (false vacuum energy) density and the plasma radiation energy density
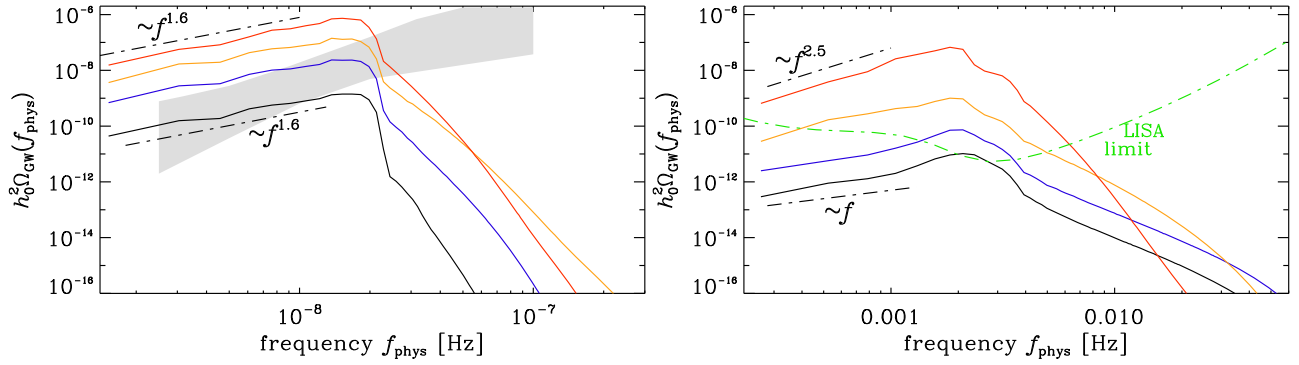
FIG. 2.   GW energy spectra (per logarithmic frequency interval), $h_0^2\Omega_{\rm GW}(f)$, for both the QCD runs a–d (left) and the EW runs A–D (right) scales shown in red, orange, blue, and black, respectively.

(which is determined at the phase transition temperature [37]). $\alpha \sim$ a few corresponds to extremely strong phase transitions. Reference [58] discusses a few beyond-SM models, which could include first-order phase transitions, and some of these models predict $\alpha \gtrsim 1$ for specific ranges of their parameter spaces. In particular, the addition of a six-dimensional term to the Higgs potential [59] or the addition of a singlet scalar field [60] allows for these particularly strong phase transitions. The induced turbulence can then be characterized by the velocity $v_i = 1/\sqrt{1 + \frac{\rho+P}{2\mathcal{E}_i}}$, which refers either to the turbulent velocity v_T or the effective Alfvén velocity v_A, and $\mathcal{E}_i$ refers to either the kinetic, $\mathcal{E}_K$, or magnetic, $\mathcal{E}_M$, energy density. By defining the efficiency coefficient $\kappa \equiv \kappa(\alpha) \in (0, 1)$ (which increases with α), i.e., the fraction of vacuum energy that is transformed into $\mathcal{E}_K$ or $\mathcal{E}_M$, rather than into heat [43], we recover *relativistic expressions* for turbulent motions, $v_T = 1/\sqrt{1 + 4/(3\kappa\alpha)}$ [61], and the Alfvén velocity, $v_A = 1/\sqrt{1 + (4/3)\rho/(2\mathcal{E}_M)}$ [62,63], while previous studies (see Ref. [45] for a review and references therein) assumed nonrelativistic motions.

The additional relativistic degrees of freedom in the early universe due to the addition of the energy densities of the turbulent sources can be subsumed into $\Delta N_{\rm eff}$.

This increase in $N_{\rm eff}$ increases the CMB-inferred value of the Hubble constant, H_0, helping to reduce the tension with late-universe values. A value of $\Delta N_{\rm eff} \sim 0.4$ could alleviate the Hubble tension [64]. Interestingly, it has been shown that the recent NANOGrav results may also favor a larger value of $N_{\rm eff}$ [65] if the signal arises in the early universe. Even though large values of α are not restricted by currently available BBN or other observational data, we limit ourselves by $\alpha_{PT} \leq 1$ that was addressed previously in several studies, see Ref. [1] and references therein.

In Fig. 2, we present GW spectra (per logarithmic frequency interval and normalized by the critical energy density) from our simulations expressed as $h_0^2\Omega_{\rm GW}(f_{\rm phys})$ for two families of models considered previously: one for the EW scale with $k/H_\star = 600$ [49] and one for the QCD phase transition with $k/H_\star = 6$ [66]. The former set of models is similar to simulations of Ref. [7], except that now we also consider models with stronger turbulent driving which is applied over one Hubble time along with a period during which the forcing decreases linearly in time to zero, again over one Hubble time.

As already noted in previous studies [7,8,49], the GW energy spectrum from forced turbulence shows a rapidly declining inertial range for frequencies above the peak. This is because only the smallest wave numbers contribute
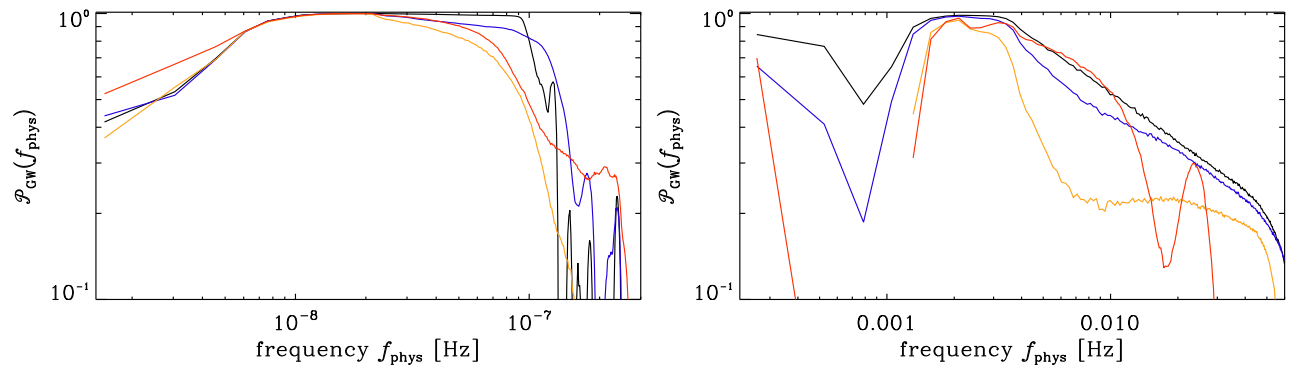
FIG. 3.   Polarization spectra, $\mathcal{P}_{\rm GW}(f)$, for the QCD runs a–d (left) and the EW runs A–D (right) scales [51] shown in red, orange, blue, and black, respectively.

significantly to the driving of GWs [49,67]. The GW energy $h_0^2 \Omega_{\rm GW}(f_{\rm phys})$ scales approximately quadratically with the ratio of magnetic energy to characteristic wave number k_0 as $(Q\mathcal{E}_M/k_0)^2$, where Q is the GW efficiency (of order unity). For the QCD phase transition, the characteristic wave number is a hundred times smaller, so the GW energy is correspondingly larger.

Toward smaller frequencies, the spectra show a shallower falloff, in some cases proportional to $f_{\rm phys}^{1.6}$. This is steeper than what has been found in earlier simulations at lower magnetic energies, but shallower than what was generally expected based on analytical considerations. Physics beyond the SM often leads to parity symmetry breaking and correspondingly to polarized gravitational waves. In Fig. 3, we show the polarization spectra, $\mathcal{P}_{\rm GW}(k) = \int 2{\rm Im}\tilde{h}_+ \tilde{h}_\times^* k^2 d\Omega_k / \int (|\tilde{h}_+|^2 + |\tilde{h}_\times|^2)k^2 d\Omega_k$, for the same runs as in Fig. 2; see also Eq. (B.17) in Ref. [68]. For the QCD phase transition with only a few bubbles per linear Hubble scale, the polarization spectra have an extended region with $\mathcal{P}_{\rm GW} \sim 1$, while for the electroweak phase transitions with tens of bubbles, the polarization spectra have nontrivial profiles with a narrower plateau.

In summary, BBN data do not limit the kinetic or magnetic energy density of the turbulence at the moment of its generation to be 10% of the radiation energy when the decay process is accounted for. Strong turbulence unavoidably results in a more powerful source for the GW signal with more optimistic prospects for GW detection.

The source code used for the simulations of this study, PENCIL CODE, is freely available from Refs. [55,56]. The simulation setups and the corresponding data are freely available from Ref. [69].

[*]tinatin@andrew.cmu.edu
[†]emmaclar@andrew.cmu.edu
[‡]jdstepp@andrew.cmu.edu
[§]brandenb@nordita.org

[1] C. Caprini and D. G. Figueroa, Classical Quantum Gravity 35, 163001 (2018).
[2] T. Kahniashvili, G. Gogoberidze, and B. Ratra, Phys. Rev. Lett. 95, 151301 (2005).
[3] S. Alexander, E. McDonough, and D. N. Spergel, J. Cosmol. Astropart. Phys. 05 (2018) 003.
[4] S. Anand, J. R. Bhatt, and A. K. Pandey, Eur. Phys. J. C 79, 119 (2019).
[5] P. Niksa, M. Schlederer, and G. Sigl, Classical Quantum Gravity 35, 144001 (2018).
[6] J. Ellis, M. Fairbairn, M. Lewicki, V. Vaskonen, and A. Wickens, J. Cosmol. Astropart. Phys. 10 (2020) 032.
[7] T. Kahniashvili, A. Brandenburg, G. Gogoberidze, S. Mandal, and A. Roper Pol, Phys. Rev. Research 3, 013193 (2021).
[8] A. Brandenburg, Y. He, T. Kahniashvili, M. Rheinhardt, and J. Schober, Astrophys. J. 911, 110 (2021).
[9] S. H. S. Alexander, M. E. Peskin, and M. M. Sheikh-Jabbari, Phys. Rev. Lett. 96, 081301 (2006).
[10] D. H. Lyth, C. Quimbay, and Y. Rodriguez, J. High Energy Phys. 03 (2005) 016.
[11] A. Lue, L.-M. Wang, and M. Kamionkowski, Phys. Rev. Lett. 83, 1506 (1999).
[12] S. Alexander and N. Yunes, Phys. Rep. 480, 1 (2009).
[13] N. Bartolo, S. Matarrese, M. Peloso, and M. Shiraishi, J. Cosmol. Astropart. Phys. 01 (2015) 027.
[14] P. Amaro-Seoane et al., Classical Quantum Gravity 29, 124016 (2012).
[15] N. Seto and A. Taruya, Phys. Rev. Lett. 99, 121101 (2007).
[16] V. Domcke, J. García-Bellido, M. Peloso, M. Pieroni, A. Ricciardone, L. Sorbo, and G. Tasinato, J. Cosmol. Astropart. Phys. 05 (2020) 028.
[17] A. Roper Pol, S. Mandal, A. Brandenburg, and T. Kahniashvili, J. Cosmol. Astropart. Phys. 04 (2022) 019.
[18] In what follows we neglect the effects of the strong primordial magnetic field on BBN dynamics as discussed in Refs. [19,20].
[19] M. Kusakabe, A. Kedia, G. J. Mathews, and N. Sasankan, Phys. Rev. D 104, 123534 (2021).
[20] Y. Lu and M. Kusakabe, Astrophys. J. Lett. 926, L4 (2022).
[21] J. A. Frieman, E. W. Kolb, and M. S. Turner, Phys. Rev. D 41, 3080 (1990).
[22] D. Grasso and H. R. Rubinstein, Astropart. Phys. 3, 95 (1995).
[23] G. M. Fuller and C. Y. Cardall, Nucl. Phys. B, Proc. Suppl. 51, 71 (1996).
[24] K. Ichikawa and M. Kawasaki, Phys. Rev. D 69, 123506 (2004).
[25] V. Simha and G. Steigman, J. Cosmol. Astropart. Phys. 06 (2008) 016.
[26] N. Sasankan, M. R. Gangopadhyay, G. J. Mathews, and M. Kusakabe, Int. J. Mod. Phys. E 26, 1741007 (2017).
[27] C. Keith, D. Hooper, N. Blinov, and S. D. McDermott, Phys. Rev. D 102, 103512 (2020).
[28] P. F. de Salas and S. Pastor, J. Cosmol. Astropart. Phys. 07 (2016) 051.
[29] B. D. Fields, K. A. Olive, T.-H. Yeh, and C. Young, J. Cosmol. Astropart. Phys. 03 (2020) 010.
[30] M. Benetti, L. L. Graef, and S. Vagnozzi, Phys. Rev. D 105, 043520 (2022).
[31] V. Simha and G. Steigman, J. Cosmol. Astropart. Phys. 08 (2008) 011.

[32] A. Vilenkin, Phys. Rev. D **22**, 3080 (1980).

[33] Y. Luo, T. Kajino, M. Kusakabe, and G. J. Mathews, Astrophys. J. **872**, 172 (2019).

[34] M. S. Turner and F. Wilczek, Phys. Rev. Lett. **65**, 3080 (1990).

[35] E. Witten, Phys. Rev. D **30**, 272 (1984).

[36] C. J. Hogan, Mon. Not. R. Astron. Soc. **218**, 629 (1986).

[37] M. Kamionkowski, A. Kosowsky, and M. S. Turner, Phys. Rev. D **49**, 2837 (1994).

[38] A. Brandenburg, K. Enqvist, and P. Olesen, Phys. Rev. D **54**, 1291 (1996).

[39] M. Christensson, M. Hindmarsh, and A. Brandenburg, Phys. Rev. E **64**, 056405 (2001).

[40] T. Kahniashvili, A. Brandenburg, A. G. Tevzadze, and B. Ratra, Phys. Rev. D **81**, 123002 (2010).

[41] A. Brandenburg, T. Kahniashvili, S. Mandal, A. Roper Pol, A. G. Tevzadze, and T. Vachaspati, Phys. Rev. Fluids **4**, 024608 (2019).

[42] R. Durrer and A. Neronov, Astron. Astrophys. Rev. **21**, 62 (2013).

[43] A. Kosowsky, A. Mack, and T. Kahniashvili, Phys. Rev. D **66**, 024030 (2002).

[44] A. D. Dolgov, D. Grasso, and A. Nicolis, Phys. Rev. D **66**, 103505 (2002).

[45] C. Caprini et al., J. Cosmol. Astropart. Phys. 03 (2020) 024.

[46] Z. Arzoumanian et al. (NANOGrav Collaboration), Astrophys. J. Lett. **905**, L34 (2020).

[47] J. Garcia-Bellido, H. Murayama, and G. White, J. Cosmol. Astropart. Phys. 12 (2021) 023.

[48] Z. Arzoumanian et al. (NANOGrav Collaboration), Phys. Rev. Lett. **127**, 251302 (2021).

[49] A. Roper Pol, S. Mandal, A. Brandenburg, T. Kahniashvili, and A. Kosowsky, Phys. Rev. D **102**, 083512 (2020).

[50] A. Brandenburg, T. Kahniashvili, S. Mandal, A. Roper Pol, A. G. Tevzadze, and T. Vachaspati, Phys. Rev. D **96**, 123528 (2017).

[51] See Supplemental Material http://link.aps.org/supplemental/10.1103/PhysRevLett.128.221301 for the full set of equations and a summary of additional parameters of the simulations.

[52] T. Vachaspati, Rep. Prog. Phys. **84**, 074901 (2021).

[53] J. Zrake and W. E. East, Astrophys. J. **817**, 89 (2016).

[54] M. Ackermann et al., Astrophys. J. Suppl. Ser. **237**, 32 (2018).

[55] A. Brandenburg et al. (Pencil Code Collaboration), J. Open Source Softwaare **6**, 2807 (2021).

[56] PENCIL CODE, 10.5281/zenodo.2315093, https://github.com/pencil-code.

[57] T. Kahniashvili, L. Kisslinger, and T. Stevens, Phys. Rev. D **81**, 023004 (2010).

[58] J. Ellis, M. Lewicki, and J. M. No, J. Cosmol. Astropart. Phys. 04 (2019) 003.

[59] D. Bodeker, L. Fromme, S. J. Huber, and M. Seniuch, J. High Energy Phys. 02 (2005) 026.

[60] J. Choi and R. R. Volkas, Phys. Lett. B **317**, 385 (1993).

[61] A. Nicolis, Classical Quantum Gravity **21**, L27 (2004).

[62] M. Gedalin, Phys. Rev. E **47**, 4354 (1993).

[63] In the nonrelativistic limit we obtain $v_T = \sqrt{2\mathcal{E}_K/(\rho + P)}$ and $v_A = B_{\mathrm{eff}}/\sqrt{4\pi(\rho + P)} = \sqrt{2\mathcal{E}_M/(\rho + P)}$.

[64] A. G. Riess et al., Astrophys. J. **826**, 56 (2016).

[65] Y. Nakai, M. Suzuki, F. Takahashi, and M. Yamada, Phys. Lett. B **816**, 136238 (2021).

[66] A. Brandenburg, E. Clarke, Y. He, and T. Kahniashvili, Phys. Rev. D **104**, 043513 (2021).

[67] A. Brandenburg, G. Gogoberidze, T. Kahniashvili, S. Mandal, A. Roper Pol, and N. Shenoy, Classical Quantum Gravity **38**, 145002 (2021).

[68] A. Roper Pol, A. Brandenburg, T. Kahniashvili, A. Kosowsky, and S. Mandal, Geophys. Astrophys. Fluid Dyn. **114**, 130 (2020).

[69] 10.5281/zenodo.5709176 (v2021.11.18); see also http://www.nordita.org/brandenb/projects/GWs-BBN/ for easier access.